


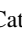




# Feature-based Characterisation of Patient-specific 3D Anatomical Models

Imon Banerjee<sup>1,2</sup> , Martina Paccini<sup>1</sup> , Enrico Ferrari<sup>3</sup> , Chiara Eva Catalano<sup>1</sup> , Silvia Biasotti<sup>1</sup> , and Michela Spagnuolo<sup>1</sup> 

<sup>1</sup>Istituto di Matematica Applicata e Tecnologie Informatiche 'E. Magenes' - CNR, Italy

<sup>2</sup>Emory School of Medicine, Atlanta, GA, USA

<sup>3</sup>Rulex Inc., Italy

## Abstract

*This paper aims to examine the potential of 3D shape analysis integrated to machine learning techniques in supporting medical investigation. In particular, we introduce an approach specially designed for the characterisation of anatomical landmarks on patient-specific 3D carpal bone models represented as triangular meshes. Furthermore, to identify functional articulation regions, two novel district-based properties are defined. The performance of both state of the art and novel features has been evaluated in a machine learning setting to identify a set of significant anatomical landmarks on patient data. Experiments have been performed on a carpal dataset of 56 patient-specific 3D models that are segmented from T1 weighed magnetic resonance (MR) scans of healthy male subjects. Despite the typical large inter-patient shape variation within the training samples, our framework has achieved promising results.*

## CCS Concepts

• **Computing methodologies** → *Shape modeling; Machine learning approaches;*

## 1. Introduction

Patient-specific 3D anatomical models (3D-PSMs) are 3D computational reconstructions of patient's anatomy, which mirror the accurate appearance of the patients' organs in the 3D space. The 3D-PSMs are expected to be extremely useful in many applications such as biomechanical simulation, computer-assisted diagnosis and surgery, prosthesis fitting, and legal medicine. However, the use of 3D-PSMs is not wide-spread yet in clinical practice because experts still prefer to rely on traditional 2D/3D medical images.

So far most of the 3D shape analysis methods developed in the Computer Graphics field [ABM\*06] are designed to analyse geometric and structural properties of the 3D models. The use of geometric descriptors to extract clinically relevant features from the 3D-PSMs is not straightforward: (i) often the anatomical features belong to regions that do not have a strong geometric characterisation; (ii) the medical definition of the features is intrinsically vague, and thus, the features cannot be coded or identified by an exact formulation; (iii) the anatomical shapes are highly variable among individuals. Moreover, the shape alteration due to pathological condition makes the anatomical shape characterisation more challenging, e.g. bone erosion induces irregular shape modification and the osteonecrosis disorder causes random collapses in the bone architecture. Finally, the interaction between different bones (like in articulations) depends on feature points that are relevant for the functional analysis of the district, but might not be geometrically

relevant on the single bone. These facts suggest that the shape analysis of the single bones should be coupled with the co-analysis of all the elements of a district with the aim of identifying interoperability properties that model the articulation functionality. In this paper, we show how a tighter integration between geometric analysis and machine-learning techniques can support the characterisation of the 3D-PSMs in terms of anatomical features. The experiments are shown on a case-study of carpal bones that has been validated by clinical experts (anatomists, radiologists, rheumatologists, surgeons). Based on the groundwork, our case-study aims to recognise a targeted set of anatomical landmarks on the 3D-PSMs of carpus, which can bring informative content to substantiate the investigation of musculoskeletal diseases (MSD), particularly Rheumatoid Arthritis (RA). The carpus is the anatomical assembly of 8 carpal bones, which constitutes one of the most complex joints of the human body. A large group of experts confirms the idea that the MSD diagnostic analyses can gain more richness if the individual carpal bone models and the district as a whole can be examined by analysing the characteristics of relevant anatomical and pathological landmarks. Moreover, the anatomical feature-based modelling can provide an enhanced understanding of patient's anatomy which can be worthwhile in several other clinical applications, e.g. biomechanical simulation, prosthesis fitting.

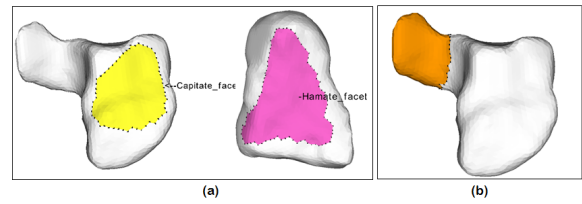
The contribution of the paper is twofold. First, we propose two novel and specialised characterisations of the carpal bones (Sec. 3.2): *Shadow map* and *Adjacency map*, which act at the level

of the anatomical district rather than on each single bone. The new characterisations will support the analysis of the carpal bones according to their functional regions (articulation and adjacency of the bones). Second, we experimented with a specific machine learning method (Sec. 4) that exploits a rich set of morphological feature vectors (state of the art purely geometric descriptors and the two new characterisations we introduced) to recognise automatically the anatomical landmarks through a machine learning approach. We have evaluated the performance of the proposed method by comparing the outcome with a fixed ground truth, i.e. a set of landmarks defined on the 3D-PSMs by an anatomist (Sec. 5.2). In the context of carpal case-study, the individual relevance of the morphological features has been evaluated by the feature ranking results derived from the proposed method, Section 5.3. Final remarks conclude the paper.

## 2. Related works

Characterising a shape means building a computational description able to preserve the most representative elements of the shape, usually a few basic types, along with their relationships and their invariants [FS98]. In this context, mathematics plays a key role to handle the complexity of digital shapes, in particular differential topology provides a setting able to formalise several problems related to shape analysis and description. In this scenario, methods have been derived to analyse the shape of an object according to the properties of real functions defined on it. The added value of these approaches is that different functions can be used according to the properties and invariants that one aims to capture, thus providing a flexible shape description framework. Examples of popular functions used in object analysis and matching are distance functions, curvature-based and geodesic-based functions, Laplace eigenfunctions and distribution maps [BDF\*08, BFF\*07]. Then, the geometric/topological information related to the shape is compactly stored into descriptors [BCA\*16], for instance, adopting feature vectors [BKS\*05], graph-based descriptions (e.g. Reeb graphs [BGSF08]), or maps [HWG14].

Unfortunately, given a collection of 3D models, a single property is not likely to provide a good organisation of the data, or at least it could be not informative enough [HZG\*12]. To address this limitation, a recent path of research aims to derive high-level information by analysing single objects in the context of larger *collections* of models: the idea is to derive information not only from the object itself, but also from its relation with the other ones in the collection [HWG14]. This is the case, for example, of the *co-segmentation* of a set of 3D objects [WAvK\*12, HFL12, KHS10], i.e. the segmentation of the objects as a whole into consistent semantic parts with part correspondences. These 3D shape analysis techniques are meant to derive *semantic* (high-level) information from low-level properties exploring their relation with the other objects in the collection [OLGM11, HZG\*12, KLM\*12, ROA\*13]. The goal is to facilitate exploration and content search as well as to understand their overall categorisation and summarise their content [LMS13]. Here *semantics* refers to the meaning, or *functionality*, of an object in a given context. The key challenge is that shapes can vary in different ways, and users may be interested in different types of variations [KLM\*12, KLM\*13]. Examples of applications



**Figure 1:** Examples of anatomical landmarks on Carpal bones : (a) articulation facets between hamate (yellow) and capitate (pink); (b) hook of hamate, prominent bony feature (orange)

are: *semantic annotation*, which is the automatic or semi-automatic labelling of objects (or parts of objects) [BAC\*16]; *attribute transfer* techniques, which study how to automatically transfer labels from a single object (or part of an object) to sets of unknown objects [KBB\*13]; the structuring of 3D large datasets to enable navigation and retrieval, which is often achieved by exploiting also the pairwise similarities between the rest of the dataset models [HSS\*13].

In all these approaches, a major issue is how to interpret such implicit knowledge. In general, the use of prior knowledge might be inevitable; anyway, the recent advances in learning techniques have achieved state-of-the-art performance in computer vision applications [CMS12]. These techniques represent a possible solution to determine automatically the weights of the different shape features on the basis of context (e.g., the shape classes of a database) [BB13, TDVC13], design class- or application-specific shape descriptors [BMM\*15] or extend deep learning techniques to geometry [MRB\*16, BBL\*17].

## 3. Morphological properties

By discussing with the domain experts, we derived that the most relevant anatomical landmarks of carpal bones in the context of MSD diagnosis and treatment are: *articulation facet* - zone of the bone that participates in articulation, *contact area* - zone of the bone that is adjacent with the neighbouring bones within the district, and *prominent bony feature* - zone of the bone that exhibits typical morphological characteristics (e.g. protrusions, concavities). Among these anatomical landmarks, frequently the articulation facets and contact areas of the carpal bones belong to a relatively flat region, while prominent bony features have peculiar morphological characteristics that are geometrically well characterised. We present the example of hamate and capitate bones in Fig. 1, where the articulation facets belong to geometric featureless regions and therefore are not well characterised via morphological properties, while the protruded bony feature - hook of hamate, can be easily described by geometric functions (e.g. distance from centre of mass).

For this reason, we decided to support the analysis of the single bones with standard geometric properties, while we drive the analysis of articulation district with the two novel properties that we introduce in Sec. 3.2. All the descriptors presented in this study have been tested on a carpal bone dataset where we have more than 100 healthy and pathological cases (affected by RA) segmented from T1 weighted Magnetic Resonance (MR) scans.

### 3.1. Bone-based properties

We have developed a 3D shape characterisation java library by implementing state-of-the-art methods for shape analysis, which we deem as relevant to the context. In the context of carpal case-study, we renamed this group of properties *bone-based*, since they are computed by considering only the shape of an individual 3D bone model. First, we consider a set of shape properties able to deal both with local and global features and can capture both intrinsic and extrinsic characteristics such as curvatures, distance functions, ratio between area and volume. Then, we selected a subset of them that can complement each other in terms of their sensitivity to feature types, and as a result, can derive high-level information useful for our application. Table 1 lists the state of the art properties that have been considered in our study, and we cite the literature where necessary. We have implemented each property as a function and we describe each model as a couple  $(X, d)$  where  $X$  is the vertex set and  $d$  is a vector that represents the value of the scalar function over  $X$ .

Our experiments with the training dataset confirmed our hypothesis that the purely geometric properties are relevant for characterising prominent bone features that are morphologically well-characterised. However, these geometric characterisation techniques are not fully suitable to identify the functional features of carpal bones that often belong to the geometric featureless and/or the flat regions.

### 3.2. District-based properties

To characterise the functional parts (articulation and contact areas) of the patient-specific 3D models, we propose two novel and specialised *district-based* properties. These measures integrate the whole district perspective with the individual shapes of the bones. The semantics behind the articulation and adjacency relations between the carpal bones has been modelled in the *Carpus ontology* [BAC\*16] which is specifically designed to support computational analysis of patient specific 3D carpal bones. We defined an ad hoc *Carpal bone Ontology* (CO) to conceptualise the anatomy of the carpus district at the granularity we needed for our application, reusing the Foundational Model of Anatomy (FMA) as much as possible [FMA]. The `FMA:Carpal_bone` and its subclasses model the 8 individual carpal bones, and the relations `CO:hasArticulationFacet` and `CO:Articulates With` model the anatomical relations between bones. In Fig. 2 the articulation relations between `FMA:Hamate` and `FMA:Capitate` are shown together with the 3D model of the entire carpal district. This formalism represents the anatomical information in a form that able to support reasoning, inference and assertion. Particularly, when such knowledge is associated directly with the patient 3D data, it allows for a dynamic navigation of the 3D geometry, with the possibility to extend the reasoning to the geometric aspects.

**Shadow map:** we introduce a novel scalar function to characterise the articulation areas of the carpal bones following the intuition that the articulation regions are the areas of the bones which *face to each other*, and these areas can be defined as the *shadow* cast by each bone onto the adjacent ones (see Fig.3). The shadow map represents this information, and this function captures not only information

on the shape of the individual bones but also about their spatial arrangement in the whole district.

The input is the eight 3D carpal bone models in the same coordinate system  $Bone[8] = \{B_1, B_2, \dots, B_8\}$  and the articulation matrix  $R[8][8]$ , which is defined by the Carpus Ontology as  $R[i][j] = 1$  when  $Bone[i]$  articulatesWith  $Bone[j]$  (Fig.2), and  $R[i][j] = 0$  otherwise. We adopt the concept of orthographic projection where the shadow is projected by a point light source and the directional light source directed opposite to the normal of the surface on which the shadow is drawn. The main idea is the following: we take the  $Bone[i]$ , and then project its approximate shadow  $S_{i,j}$  on another bone surface  $Bone[j]$  which is defined by a generalised cone  $C_{i,j} \subset R^3$  that marks the maximum region of space compatible with  $Bone[j]$  and  $Bone[i]$  (see Fig. 3). Note that the shadow of  $Bone[i]$  is projected onto  $Bone[j]$  only if  $R[i][j] = 1$ .

Following this approach, we compute the *ShadowMap*[8] vector was output, which describes the shadows projected onto all the eight carpal bones. Algorithm 1 presents the pseudo-code to compute the *Shadow Map* from the carpal bones.

---

#### Algorithm 1 Shadow map computation

---

```

1: procedure SHADOW MAP COMPUTATION (BONES[8])
2:   Input: Bones[8]  $\leftarrow$  8 carpal bone triangulations (.off)
3:   R[8][8]  $\leftarrow$  Articulation Matrix
4:   Output: ShadowMap[8]  $\leftarrow$  array of scalar values
5:   for  $\langle i = 1 \text{ to } 8 \rangle$  do
6:     for  $\langle j = 1 \text{ to } 8 \rangle$  do
7:       if ( $i \neq j$  and  $R[i][j] = 1$ ) then
8:         Shadow[ $i$ ]  $\leftarrow$  PROJECTION(Bone[ $i$ ], Bone[ $j$ ])
9:         DrawContour(Shadow[ $i$ ])  $\triangleright$  contour based on the
           pre-defined range
10:  procedure COMPUTESHADOW(Model1, Model2)
11:    KDTree  $\leftarrow$  BuildKDTree(Model2)
12:    for each vertex $k$  of Model1 do
13:      CloseP  $\leftarrow$  FindClosestPoint(vertex $k$ , KDTree)
14:      SquareDis  $\leftarrow$  EuclideanDistance(vertex $k$ , CloseP)
15:      if SquareDis < Shadow[ $i$ ][ $k$ ] then
16:        Shadow[Model1][ $k$ ]  $\leftarrow$  SquareDis

```

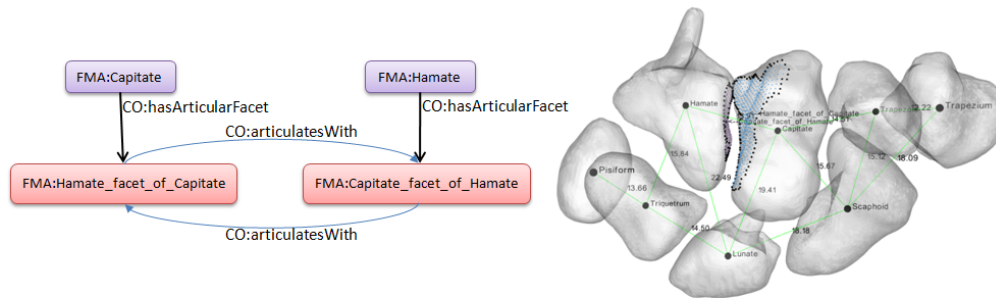
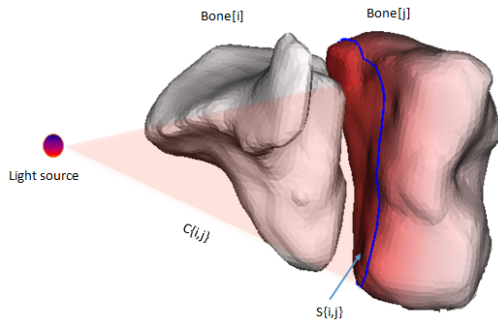
---

We present results of the *Shadow map* computation in Fig. 4 (healthy and pathological dataset), where the bone surfaces are coloured according to the triangle-wise scalar value of the *ShadowMap* function and the contours are drawn based on a predefined scalar value range. In order to validate our approach we have also performed experiments on the models segmented from different acquisitions methods: computer tomography (CT) and magnetic resonance imaging (MRI), and in both cases the characterisation of the articulation regions conform to their expected location (Fig. 4). In the figure, we also represent the shadow map computation on a pathological dataset (RA stage 3) where, regardless of the fact that the bone surfaces are mostly eroded, the descriptor provides an acceptable characterisation by coupling the bone geometry with the spatial arrangement.

However, the *Shadow map* fails to produce a reasonable characterisation solely when the spatial arrangement of the district is

**Table 1:** Bone-based properties - a list of state-of-the-art methods experimented in our study

Characterisation of a single bone	
<i>Distance-based</i>	
Distance from the centre-of-mass (CM)	Spatial distribution of the object with respect to its centre of mass (barycentre).
Distance from a principal axis (LD) [BB13]	Spatial distribution of the object with respect to its main axis.
Distance from a principal plane (PD) [BB13]	Surface symmetry with respect to the plane through the bary-centre and with the principal axis as its normal vector.
Distance from the convex-hull (CV)	Punctual distance between the shape vertices and the object convex-hull (crumpliness [CRC*02]).
Geodesic distance from random surface samples (GD) [HSKK01]	Average geodesic distance where the source points are randomly distributed.
Geodesic distance with the farthest point sampling (GD_FD) [MD03]	Average geodesic distance where the source points are distributed sampling algorithm.
<i>Curvature-based</i>	
Gaussian Curvature (GC) [PS06]	Product of the principal curvatures.
Mean Curvature (MC) [PS06]	Half the sum of the principal curvatures.
Shape Index (SI) [KvD92]	Ratio between Gaussian and Mean curvatures.
<i>Spectral-based</i>	
3rd, 4th, 6th and 7th Eigen vectors [PP93]	3rd,4th, 6th and 7th Eigen vectors computed from the Eigen decomposition of Laplace-Beltrami operator.

**Figure 2:** Conceptualisation of the *articulatesWith* relation in the Carpus Ontology on the left, Corresponding visualisation on the 3D model on the right**Figure 3:** The shadow map descriptor represents the shadow projected from a bone on its adjacent one. The directional light source is opposite to the normal of the surface on which the shadow is drawn

significantly altered due to some typical pathological conditions, e.g. advanced carpal collapse, missing bone, complex fracture.

**Inter-bone Adjacency graph and Adjacency map:** the Inter-bone Adjacency graph is a 3D graph that represents the inter-carpal adjacency. It has been defined by the following idea: if in the Carpus ontology the `FMA:Capitate` bone has relation `CO:adjacentWith` with the `FMA:Hamate`, there is an edge

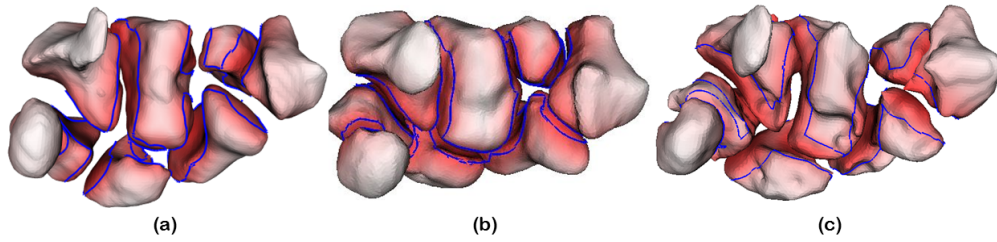
connecting the centroid of the capitate and hamate models. Therefore, in the Inter-bone Adjacency graph, the nodes are defined by the bone centroids, and an arc exists between a pair of nodes if the respective bones are adjacent to each other in the joint setting. Based on this conceptual graph, we can represent the inter-bone distance as the edge weight in the articulation graph. In Figs. 5.a, we show the computation result of an Inter-bone Adjacency graph where the edge weights are represented in mm.

In this study the Inter-bone Adjacency graph is utilised to compute the second district-based descriptor: the *Adjacency Map*. The Adjacency map characterises the adjacent surfaces of each bone on the basis of the inter-carpal adjacency relations. The idea behind this is to compute the minimum geodesic distance map for each bone surface, where the sources are the intersection points between the bone models and the inter-bone articulation graph.

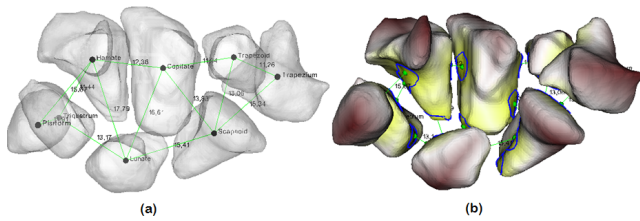
Formally, the *AdjacencyValue* of the  $i$ th vertex in a bone model can be computed as:  $AdjacencyValue_i = \min[d(v_i, s_1), d(v_i, s_2), \dots, d(v_i, s_n)]$ , where  $v_i$  is the  $i$ th vertex,  $s_j$  is the  $j$ th source, and  $d(v, s)$  is the geodesic distance between the vertex  $v$  and source  $s$ . If a bone has adjacency with three other bones, as in the case of hamate, then  $n = 3$ . In Fig. 5.b., the green points represent the intersecting points, and the yellow colour identifies the regions with the minimum geodesic distance, which indicates the adjacent regions.

Similar to the Shadow map, the Adjacency map can successfully

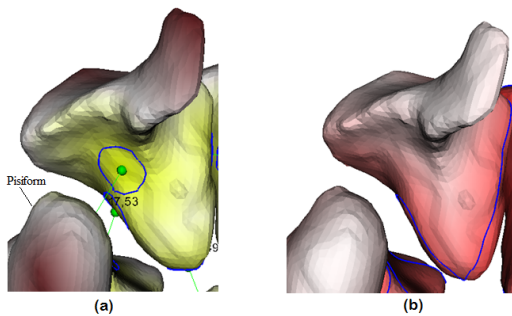




**Figure 4:** The computation of the Shadow Map applied on: (a) models segmented from MRI images; (b) models segmented from CT images; (c) a pathological case affected by rheumatoid arthritis stage 3 (pinker areas indicates higher values of the shadow map)



**Figure 5:** (a) An example of Inter-bone Adjacency graph, which represents the relations of the articulations between the carpal bones, and the weight of the arc is the inter-bone distance, and (b) An example of Adjacency map computed on a carpal district: the distance from the centre of mass increases from yellow to brown



**Figure 6:** A patient-specific hamate bone characterised by the (a) Inter-bone Adjacency map with the pisiform, and (b) the Shadow map of the hamate on the pisiform

be used as a tool to explore hidden structures and subtle kinematics of carpal joints. The main difference with the Shadow map is that the Adjacency map is defined according to the inter-carpal *adjacency* relations and aims to recognise the adjacent areas of the carpal bones, while the Shadow map considers the *articulation* relations, and is designed to characterise articulation facets. To distinguish better the two characterisation functions, we show an example of a facet of hamate bone in Fig. 6 where the characterisations of Adjacency map and Shadow map differ significantly, since the hamate has *adjacency* relation with the pisiform bone, but does not *articulate* with it in normal conditions.

#### 4. Automatic detection of landmarks

We designed a method that automatically detects the anatomical landmarks by exploiting the morphological features of the patient-specific 3D data. To identify the landmarks, our method uses the Logic Learning Machine model (see Sec. 4.2). This technique belongs to the family of machine learning, a class of algorithms designed to extract information from the data without any *a priori* assumptions. In this specific context, a *classification* problem is to be solved: the objective consists in labelling each example, i.e. each vector of input features, with an output class, namely the landmark associated with each vertex.

To improve the quality and the readability of the model, a different classification problem was considered for each of the 8 bones involved in the district. Therefore, each classification problem can be formulated as the computation of a function  $f: X \rightarrow I_{m_j}$ , where  $X_j$  is the input space (i.e. the vertices of the 3D models for the  $j$ -th bone) and  $I_{m_j}$  is the set of  $m_j$  possible classes associated with the  $j$ -th bone ( $m_j - 1$  is the number of anatomical landmark to be identified and "no landmark" is an extra class).

##### 4.1. Dataset

The dataset employed for the tests contains 56 patient-specific carpal bone models segmented from T1 weighted MR images belongs to healthy male subjects<sup>†</sup>. Using the interactive tool SemAnatomy3D [BAC\*16], the 56 3D models have been manually annotated, the number of landmarks for each model depends on the type of bone. The number of landmarks per model is in the range 3 (Pisiform) - 8 (Capitate) with a total number of 45 landmarks per district. The regions mostly represented are the prominent bony features and articulation facets. The landmarks are represented as areal features of the 3D mesh. We have computed all the 13 state of the art properties (see Table 1) and the 2 novel ones for all the 56 bones in our dataset.

Finally, each bone consists of the following three components, and each component is represented in a matrix form to be fetched in the machine learning system:

1. **Geometry** - contains the vertex coordinates  $(x, y, z)$  that is extracted from the .OFF file of the 3D model. The dimension of

<sup>†</sup> [http://visionair.ge.imati.cnr.it/medical/browse\\_medical.zul](http://visionair.ge.imati.cnr.it/medical/browse_medical.zul)

the matrix is  $n \times 3$ , where  $n$  is the number of vertex in the bone model. On average, each bone model contains 5000 - 7000 vertices.

2. **Annotation** - contains annotation labels corresponding to each vertex. Up to now, we assume that a vertex can only have a single annotation. The dimension of the matrix is  $n \times 1$ , where  $n$  is the number of vertex in the bone model, and a string represents the annotation tag. If the vertex does not belong to any annotated region, we associate the "no landmark" tag. On average, 10 - 12 anatomical landmarks are listed for each carpal bone, and in total 64 anatomical landmarks are catalogued for the whole carpal district.
3. **Feature vector** - contains the scalar values of the feature vectors computed for each vertex. The dimension of the matrix is  $n \times d$ , where  $n$  is the number of vertex, and  $d$  is the number of feature vectors, 15 in our case.

#### 4.2. Formulation of the model

The final data matrix containing the geometry, the feature vector and the annotation for each vertex of the training set is used to build a model able to give the correct output (annotation) in correspondence of a given input vector (geometry and features). Several approaches have been proposed for classification: some of the most known are Multilayer Perceptrons, Support Vector Machines, and k-Nearest Neighbor. The literature on the machine learning is very vast and we cannot be discussed extensively here; for recent surveys on this topic the reader can refer to [BG16,PSY\*18]. However, most of the techniques for classification are not able to provide useful insight of the data: in other words, they are able to forecast an output value given an input vector, but they are not able to explain the reasons of this prediction. On the contrary, in this context it is essential not only to have a good prediction but also to improve the level of knowledge on the studied system. For this reason, we have preferred an approach based on rules, namely the *Logic Learning Machine (LLM)*, an efficient implementation of the Switching Neural Network model [Mus05]. LLM presents some advantages with respect to Decision Tree (DT) [Utg89], the other well known method for rule generation. One of the most important advantages is the possibility of generating sets of rules that reveal different points of view on the data, which allow the identification of the most important features. Moreover, the performances of LLM with respect to DT are usually higher. LLM is included in RuleX Analytics, a software suite developed and commercialised by RuleX Inc (<http://www.rulex.ai/>). Briefly, the classifier generated by LLM is described by a set of intelligible rules of the type:

**if** premise **then** consequence

where premise is a logical product (AND) of conditions on the components of the input vector  $x$ , and consequence provides a class assignment for the output. LLM is trained through an optimised version of the *Shadow Clustering (SC)* [MF11] algorithm, a rule generation technique based on Boolean function synthesis. SC adopts an aggregating policy: at any iteration some patterns belonging to the same output class are grouped to produce an intelligible rule. A suitable heuristic approach is employed to generate rules exhibiting the highest covering (i.e. the percentage of cases a rule is able to describe) and the lowest error; a trade-off between

**Table 2:** The properties of the rules generated for each bone

Bone	# rules	Average # conditions	Average covering	Average error
Capitate	91	5.26	12.0	0.89
Hamate	70	5.10	18.6	0.91
Lunate	86	5.24	13.7	0.93
Pisiform	44	4.86	13.9	0.90
Scaphoid	79	5.47	15.0	0.94
Trapezium	61	5.08	15.1	0.88
Trapezoid	68	5.35	15.1	0.91
Triquetrum	52	4.81	17.0	0.91

these two different objectives generally leads to final models with a good accuracy. In these tests error for each rule was forced to be lower than 1%. Clustering examples of the same landmark permits to extract knowledge regarding similarities about the members of a given class rather than information about their differences.

Moreover, another interesting property of the approach is the possibility of deriving a ranking of the features according to their relevance in discriminating the landmarks. This feature ranking is not a measure of the bi-variate correlation between the input and the output, but rather a measure of the contribution of the features inside the set of rules. The relevance of a feature in a set of rules is evaluated according to these criteria:

- the covering of the rules in which the feature is present;
- the importance of the condition associated with the feature inside the rule, evaluated by considering the increase of error that the elimination of this condition would lead to.

By considering all the rules, the global relevance of the feature in the set of rules can be computed; moreover, also relevances related to each landmark can be obtained in the same way.

## 5. Experimental results

To assess the effectiveness of the learning model described in Section 4.2 we adopted a leave-one-out cross-validation strategy, which is expected to mitigate over-fitting and gives a reasonable score even in case the number of elements is quite limited, as in our use case (see Section 4.1). In practice, the model obtained using all the patients but one (the training set corresponds to the carpal district of 6 patients), was tested on the data of the remaining patient (the test set correspond to a single patient). The role of the test and the training set is assigned in rotation and then, the performance scores are averaged.

### 5.1. Generation of the set of rules

The data given in input to the LLM include spatial coordinates, standard descriptors and novel features. Then, the LLM was run to get a set of rules for each of the 8 bones of the district. The training of LLM takes few minutes (from 30 to 180 seconds on a standard PC with i7 2.4GHz processor and 8 GB of RAM): it leads to 8 sets of rules that are described in the Table 2, where all the features are considered.

To understand better the results let us consider a rule regarding Capitate.

```

if  $4.262 < \text{Centre of Mass} \leq 7.067$ 
  AND  $X \text{ position} \leq 0.51$ 
  AND  $\text{Distribution Map} \leq 7.624$ 
then Landmark = Hamate facet of Capitate

```

This rule characterises some points of the landmark “Hamate facet of Capitate”. Its covering is 50.3%: it means that the 50.3% of the “Hamate facet of Capitate” points are described by this rule. On the contrary, its error is 0.98%: this means that the rule is satisfied also by 0.98% of the cases of other landmarks. Allowing a (small) amount of error is a good practice to avoid overfitting: this happens when the classifier performs very well on the data of the training set (in case affected by noise) but it is not able to generalise on the test set.

The quality of the rules depends on the characterisation of the landmark: if a landmark is well defined, then few rules are enough to describe it; otherwise, more low quality rules are needed. For example, the “No landmark” points are very scattered in every bone and indeed many rules with rather low covering are needed to describe them.

## 5.2. Accuracy of the anatomical landmark detection

First, we assessed the performance of the proposed method concerning the capability of recognising the targeted set of anatomical landmarks on the 3D-PSMs. This is done by verifying the truthfulness of the outcomes of our method by comparing with the ground truth created by the medical doctors. The ground truth was created by an anatomist who was asked to annotate a specific set of anatomical landmarks (42 areal patches) on the patient-specific 3D carpal models (8 carpal bones) by using SemAnatomy3D. The expert was assisted also by the visualisation of the original MRI image stack ( $256 \times 256 \times 52$ ) side-by-side, which originated the 3D-PSMs. Afterwards, we identified the targeted set of anatomical landmarks on the same dataset.

According to the experts, the correctness of the location of anatomical landmarks is more relevant than detecting smooth boundaries of the segments. This implies that the number of landmarks identified may be considered a measure of success. Thus, we decided to follow a region-based approach and evaluate the difference between the ground truth and the automatic outcome by computing the following measures: **Correct area**: the area that is marked with the same annotation as in the ground truth; **False-negative area**: the area which is marked as landmark region in the ground truth, but detected as no landmark region by the automatic method; **False-positive area**: the area which is marked as no landmark in the ground truth, detected as landmark by the automatic method. Indeed, a low number of false negative and false positive is an indicator of the accuracy of the algorithm. Due to inter-patient shape variability, experiencing error in automatic landmark detection process is quite probable, and we must choose which side to err towards. Most of the experts involved in our study remarked that having a higher false positive rate is better than higher false negative rate.

Given this hypothesis, Fig. 7 presents the outcomes of our

method on four distinct carpal bones of patient X (unknown test case), displayed along with the ground truth. The last row of Fig. 7 presents the results where the automatic annotation has been matched with the ground truth, and the surface has been coloured according to: (a) correct landmark prediction - green, (b) correct no landmark prediction - pink, (c) false-positive - yellow, (d) false-negative - red. Finally, we measured the areas to evaluate quantitatively the performance: the method has achieved 78% overall accuracy.

The experimental observation points to the fact that the proposed method considers only certain morphological rules which depends on bone-based properties, and therefore it is sensitive to inter-patient shape variations and noise. However, this method could be helpful to highlight certain pathological anomalies related to the bone morphology (e.g. erosion, bone growth).

## 5.3. Ranking the feature properties

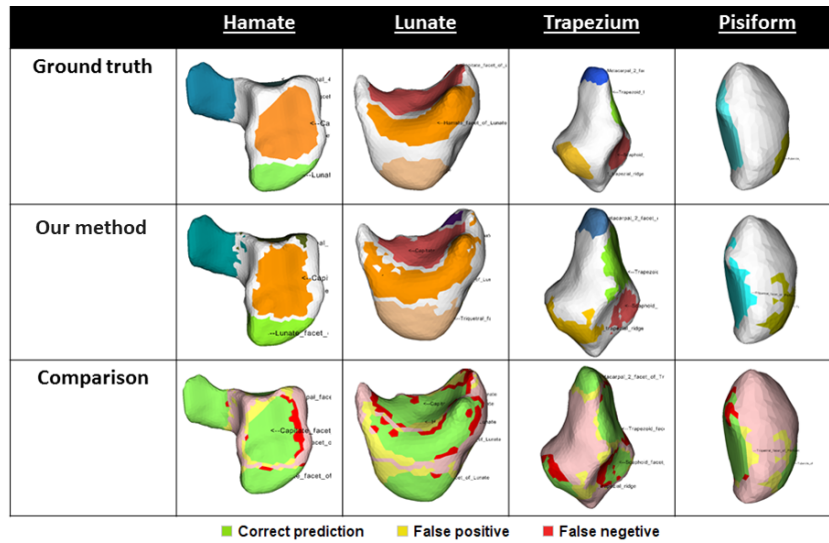
We present a statistical summary of the feature ranking derived from the LLM training setting, and discuss a set of interesting examples of carpal landmarks.

In Fig. 8, we represent the overall LLM feature ranking for each individual descriptor. According to the results, among 42 anatomical landmarks of carpal bones, the 2 distinct district-based properties (Shadow map and Adjacency map) are discriminative for 26 landmarks, while 16 landmarks are detected by the 14 standard geometric properties (Table 1). According to the overall numerical relevance in the carpal anatomical landmark detection task, Shadow map and Adjacency map are accessed individually as more discriminative than the descriptors listed in Table 1.

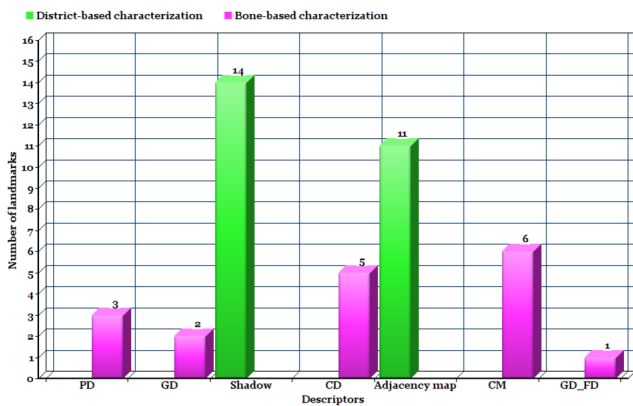
This result supports the fact that the two novel district-based properties are not only efficient in characterising the carpal district in terms of functional regions, but also performs robustly against the inter-patient shape variations. As seen from the chart, curvature-based descriptors have not been considered as significant for the anatomical landmark detection task. The result shows that the distance-based descriptors (e.g. distance from centre of mass, distance from convex hull, geodesic distance) offer a more stable characterisation of patient-specific carpal bones than the curvature-based descriptors, which highlight only the local features.

Afterwards, we analysed the feature ranking for individual anatomical landmarks, which confirm the fact that the district-based properties can efficiently characterise the functional facets of carpal bones, often belonging to geometric featureless and/or flat regions. We observed another interesting characteristic of the district-based properties: they frequently recognise not only one but a set of functional facets which are isolated area in the 3D model. For instance, the Shadow map appears to be the most discriminative descriptor for detecting the articulation facets of the hamate bone (with capitate and triquetral), although such articulation facets are mostly flat and located almost in the opposite facets of the hamate bone (Fig. 9). Similarly, the Shadow map is discriminative for the lunar facet of the scaphoid bone (Fig. 10, where also the confusion matrix is represented).

Oppositely, most of the prominent bony features were characterised by the standard geometric properties. The latter work well



**Figure 7:** Comparison between annotations related to 4 bones: in the top row the groundtruth (annotations performed by experts), in the middle the outcome of our method, and in the bottom the corresponding annotations overlapped on the same bone



**Figure 8:** Feature ranking: each histogram bar represents how many times each descriptor was discriminative for the landmark recognition. The descriptor acronyms are derived from Table 1

also for some relatively small sized peculiar shaped bone (e.g. lunate) where the articulation facets are located close to each other, and therefore are difficult to be detected via the district-based properties. In that case, standard geometric properties become more relevant for detecting the articulation facets, particularly when the landmarks exhibit some specific geometric characteristics. For instance, the facet of the lunate bone which articulates with the capitate is located in the distal surface, which has a deep concavity for the specific conformation of the lunate (see Fig. 11). In the LLM feature ranking for this facet, distance from convex hull feature vector (CD) is ranked as top relevant among the others which is well-aligned with our expectations.

In contrast to the capitate facet, the hamate, scaphoid and tri-

quetrum facet of the lunate do not have any specific geometric characteristics that are consistent across the training samples (Fig. 12). Therefore, the standard geometric properties fail. Moreover, these facets are positioned relatively far to each other: this fact suggests that the district-based characterisation is more suitable for this case capturing better the structure of the carpal region. As expected, the Adjacency map rates as most relevant for these facets by the LLM algorithm.

Another interesting example is the hook of the hamate which is not an articulation facet but a prominent feature, where the Shadow map is prominent and stable enough to be rated over the standard geometric characterisations (Fig. 9). We explain this by observing that the hook of the hamate is a region which is not adjacent to any other carpal bones and the Shadow map describes that region as an area where no shadow appears.

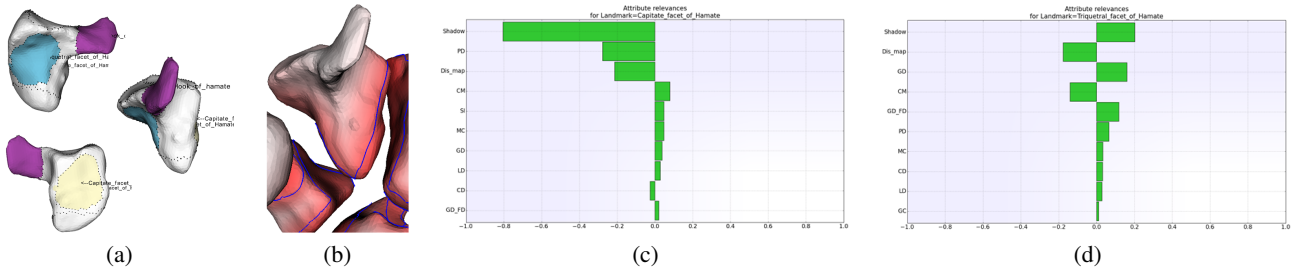
**6. Concluding remarks**

We proposed a hybrid approach based on geometric analysis and machine-learning that can support the characterisation of the 3D-PSMs of carpal bones in terms of significant anatomical features. We approached the problem by capitalising the existing shape analysis methods and devising novel district-based descriptors specific for the considered case-study. Nevertheless, a similar approach can be adopted for other anatomical districts, targeting different pathologies.

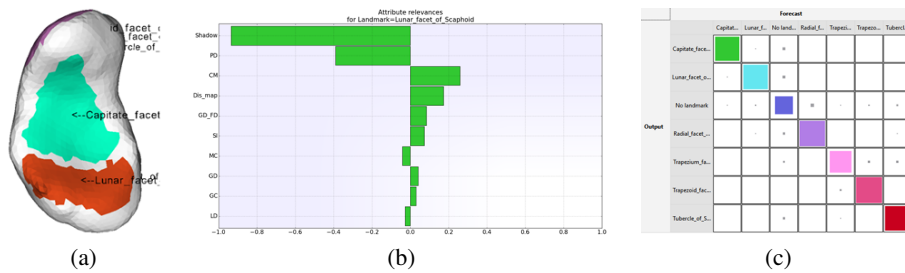
Further analysis and statistics could be computed in the future considering various patients’ datasets and engaging a group of experts for creating a richer *ground truth*. A statistically relevant analysis with a bigger training set could bring more interesting and legitimate insights about the performance of the whole framework.

The presented research has been primarily conducted to demonstrate the potential of using specialised morphological descriptors

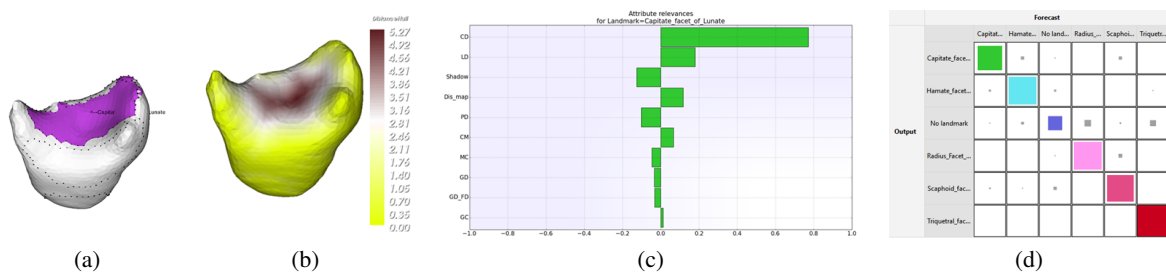




**Figure 9:** An example of annotated hamate bone: (a) annotated capitate facet (white), hook of hamate (violet) and triquetral facet (blue); (b) the corresponding shadow map; (c) the feature ranking in the identification of the capitate facet of hamate area: the shadow map is the most discriminative in that it does not generally intervene in the identification of that facet; (d) feature ranking in the identification of the triquetral facet of hamate: the shadow map is the most discriminative but in the opposite sense, since it is the descriptor that intervene the most.



**Figure 10:** (a) An example of the lunar facet of the scaphoid bone (brown); (b) the feature ranking derived by the LLM algorithm; (c) the confusion matrix of the results compared to the ground truth.



**Figure 11:** (a) An example of the capitate facets of lunate; (b) the computation of the distance from convex hull; (c) the feature ranking derived by LLM algorithm (d) the confusion matrix of the results compared to the ground truth

to interpret patient-specific 3D models which could be relevant for clinical study. The promising results achieved by this study highlights the benefits of conducting more interdisciplinary research in this direction.

**References**

[ABM\*06] ATTENE M., BIASOTTI S., MORTARA M., PATANÉ G., SPAGNUOLO M., FALCIDIENO B.: Computational methods for understanding 3d shapes. *Computers & Graphics* 30, 3 (2006), 323–333.

[BAC\*16] BANERJEE I., AGIBETOV A., CATALANO C. E., PATANÉ G., SPAGNUOLO M.: Semantics-driven annotation of patient-specific 3d data: a step to assist diagnosis and treatment of rheumatoid arthritis. *The visual computer* 32 (2016), 1337–1349.

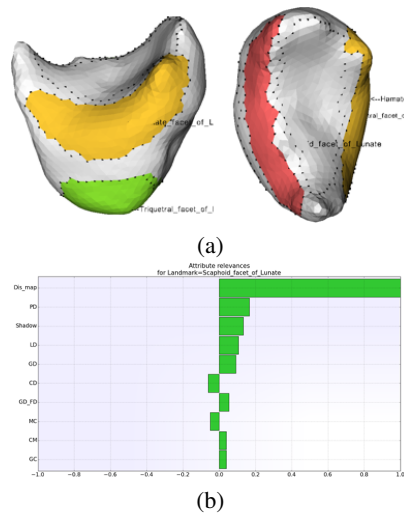
[BB13] BARRA V., BIASOTTI S.: 3D shape retrieval using kernels on extended reeb graphs. *Pattern Recognition* 46, 11 (2013), 2985–2999.

[BBL\*17] BRONSTEIN M. M., BRUNA J., LECUN Y., SZLAM A., VANDERGHEYNST P.: Geometric deep learning: Going beyond euclidean data. *IEEE Signal Process. Mag.* 34, 4 (2017), 18–42.

[BCA\*16] BIASOTTI S., CERRI A., AONO M., HAMZA A. B., GARRO V., GIACHETTI A., GIORGI D., GODIL A., LI C., SANADA C., SPAGNUOLO M., TATSUMA A., VELASCO-FORERO S.: Retrieval and classification methods for textured 3D models: a comparative study. *The Visual Computer* 32, 2 (2016), 217–241.

[BDF\*08] BIASOTTI S., DE FLORIANI L., FALCIDIENO B., FROSINI P., GIORGI D., LANDI C., PAPALEO L., SPAGNUOLO M.: Describing shapes by geometrical-topological properties of real functions. *ACM Comput. Surv.* 40, 4 (2008), 1–87.

[BFF\*07] BIASOTTI S., FALCIDIENO B., FROSINI P., GIORGI D., LANDI C., PATANÉ G., SPAGNUOLO M.: 3D shape description and matching based on properties of real functions. In *Eurographics 2007, Tutorial Notes* (2007), pp. 949–998.



**Figure 12:** An example of annotated lunate bone: (a) the hamate facet (yellow), the scaphoid facet (red) and triquetrum facet (green); (b) the LLM feature ranking for the scaphoid facet of lunate: in this example the the distance map is largely the most discriminative descriptor

- [BG16] BUCZAK A. L., GUVEN E.: A survey of data mining and machine learning methods for cyber security intrusion detection. *IEEE Communications Surveys & Tutorials* 18 (2016), 1153–1176.
- [BGSF08] BIASOTTI S., GIORGI D., SPAGNUOLO M., FALCIDIENO B.: Reeb graphs for shape analysis and applications. *Theoretical Computer Science* 392, 1–3 (2008), 5–22. doi: 10.1016/j.tcs.2007.10.018.
- [BKS\*05] BUSTOS B., KEIM D. A., SAUPE D., SCHRECK T., VRANIĆ D. V.: Feature-based similarity search in 3D object databases. *ACM Computing Surveys* 37, 4 (December 2005), 345–387.
- [BMM\*15] BOSCAINI D., MASCI J., MELZI S., BRONSTEIN M. M., CASTELLANI U., VANDERGEHYNST P.: Learning class-specific descriptors for deformable shapes using localized spectral convolutional networks. *Comput. Graph. Forum*, 35 (2015).
- [CMS12] CIRESAN D., MEIER U., SCHMIDHUBER J.: Multi-column deep neural networks for image classification. In *Computer Vision and Pattern Recognition, IEEE Conference on* (2012), pp. 3642–3649.
- [CRC\*02] CORNEY J., REA H., CLARK D., PRITCHARD J., BREAKS M., MACLEOD R.: Coarse filters for shape matching. *IEEE Computer Graphics and Applications* 22, 3 (May 2002), 65–74.
- [FMA] Foundational model of anatomy. <http://sig.biostr.washington.edu/projects/fm/AboutFM.html>.
- [FS98] FALCIDIENO B., SPAGNUOLO M.: A shape abstraction paradigm for modeling geometry and semantics. In *Proceedings of the Computer Graphics International 1998* (Washington, DC, USA, 1998), CGI '98, IEEE Computer Society, pp. 646–656.
- [HFL12] HU R., FAN L., LIU L.: Co-segmentation of 3D shapes via subspace clustering. In *SGP'12: Proceedings of the 2012 Eurographics Symposium on Geometry Processing* (2012), pp. 1703–1713.
- [HSKK01] HILAGA M., SHINAGAWA Y., KOHMURA T., KUNII T. L.: Topology matching for fully automatic similarity estimation of 3D shapes. In *Conference on Computer Graphics and Interactive Techniques (SIGGRAPH)* (2001), ACM, pp. 203–212.
- [HSS\*13] HUANG S.-S., SHAMIR A., SHEN C.-H., ZHANG H., SHEFFER A., HU S.-M., COHEN-OR D.: Qualitative organization of collections of shapes via quartet analysis. *ACM Transactions on Graphics* 32, 4 (July 2013), 71:1–71:10.
- [HWG14] HUANG Q., WANG F., GUIBAS L.: Functional map networks for analyzing and exploring large shape collections. *ACM T. Graphic.* 33, 4 (2014), 36:1–36:11.
- [HZG\*12] HUANG Q.-X., ZHANG G.-X., GAO L., HU S.-M., BUTSCHER A., GUIBAS L.: An optimization approach for extracting and encoding consistent maps in a shape collection. *ACM T. Graphic.* 31, 6 (2012), 167:1–167:11.
- [KBB\*13] KOVNATSKY A., BRONSTEIN M. M., BRONSTEIN A. M., GLASHOFF K., KIMMEL R.: Coupled quasi-harmonic bases. *Computer Graphics Forum* 32, 2pt4 (2013), 439–448.
- [KHS10] KALOGERAKIS E., HERTZMANN A., SINGH K.: Learning 3D mesh segmentation and labeling. *ACM Trans. Graph.* 29 (July 2010), 102:1–102:12.
- [KLM\*12] KIM V. G., LI W., MITRA N. J., DIVERDI S., FUNKHOUSER T.: Exploring collections of 3D models using fuzzy correspondences. *ACM T. Graphic.* 31, 4 (2012), 54:1–54:11.
- [KLM\*13] KIM V. G., LI W., MITRA N. J., CHAUDHURI S., DIVERDI S., FUNKHOUSER T.: Learning part-based templates from large collections of 3d shapes. *ACM T. Graphic.* 32, 4 (2013), 70:1–70:12.
- [KvD92] KOENDERINK J. J., VAN DOORN A. J.: Surface shape and curvature scales. *Image and vision computing* 10, 8 (1992), 557–564.
- [LMS13] LAGA H., MORTARA M., SPAGNUOLO M.: Geometry and context for semantic correspondences and functionality recognition in man-made 3D shapes. *ACM T. Graphic.* 32, 5 (Oct. 2013), 150:1–150:16.
- [MD03] MOENNING C., DODGSON N. A.: Fast marching farthest point sampling. In *Proc. EUROGRAPHICS* (2003).
- [MF11] MUSELLI M., FERRARI E.: Coupling logical analysis of data and shadow clustering for partially defined positive boolean function reconstruction. *IEEE Transactions on Knowledge and Data Engineering* 23, 1 (2011), 37–50.
- [MRB\*16] MASCI J., RODOLÀ E., BOSCAINI D., BRONSTEIN M. M., LI H.: Geometric deep learning. In *SIGGRAPH ASIA 2016, Macao, December 5-8, 2016 - Courses* (2016), Mitra N. J., (Ed.), ACM, pp. 1:1–1:50.
- [Mus05] MUSELLI M.: Switching neural networks: A new connectionist model for classification. In *Neural Nets*. Springer, 2005, pp. 23–30.
- [OLGM11] OVSIJANIKOV M., LI W., GUIBAS L., MITRA N. J.: Exploration of continuous variability in collections of 3d shapes. *ACM T. Graphic.* 30, 4 (2011), 33:1–33:10.
- [PP93] PINKALL U., POLTHIER K.: Computing discrete minimal surfaces and their conjugates. *Experimental mathematics* 2, 1 (1993), 15–36.
- [PS06] POLTHIER K., SCHMIES M.: Straightest geodesics on polyhedral surfaces. In *ACM SIGGRAPH 2006 Courses* (New York, NY, USA, 2006), SIGGRAPH '06, ACM, pp. 30–38.
- [PSY\*18] POUYANFAR S., SADIQ S., YAN Y., TIAN H., TAO Y., REYES M. P., SHYU M.-L., CHEN S.-C., IYENGAR S. S.: A survey on deep learning: Algorithms, techniques, and applications. *ACM Comput. Surv.* 51, 5 (Sept. 2018), 92:1–92:36.
- [ROA\*13] RUSTAMOV R. M., OVSIJANIKOV M., AZENCOT O., BEN-CHEN M., CHAZAL F., GUIBAS L.: Map-based exploration of intrinsic shape differences and variability. *ACM T. Graphic.* 32, 4 (2013), 72:1–72:12.
- [TDVC13] TABIA H., DAOUDI M., VANDEBORRE J.-P., COLOT O.: A parts-based approach for automatic 3D shape categorization using belief functions. *ACM Trans. Intell. Syst. Technol.* 4, 2 (2013), 33.
- [Utg89] UTGOFF P. E.: Incremental induction of decision trees. *Machine Learning* 4, 2 (Nov 1989), 161–186.
- [WAvK\*12] WANG Y., ASAFI S., VAN KAICK O., ZHANG H., COHEN-OR D., CHEN B.: Active co-analysis of a set of shapes. *ACM Transactions on Graphics* 31, 6 (Nov. 2012), 165:1–165:10.